Using the Sol–Gel-Derived CuO/CuAl2O4 Oxygen Carrier in Chemical Looping with Oxygen Uncoupling for Three Typical Coals

ARTICLE *in* ENERGY & FUELS · APRIL 2013

Impact Factor: 2.79 · DOI: 10.1021/ef3021602

4 AUTHORS, INCLUDING:

Daofeng Mei
Huazhong University of Science and Technology
15 PUBLICATIONS **91** CITATIONS
SEE PROFILE

Haibo Zhao
Huazhong University of Science and Technology
119 PUBLICATIONS **902** CITATIONS
SEE PROFILE

energy&fuels

Article

pubs.acs.org/EF

Using the Sol–Gel-Derived $CuO/CuAl_2O_4$ Oxygen Carrier in Chemical Looping with Oxygen Uncoupling for Three Typical Coals

Daofeng Mei, Haibo Zhao,* Zhaojun Ma, and Chuguang Zheng

State Key Laboratory of Coal Combustion, Huazhong University of Science and Technology (HUST), Wuhan 430074, People's Republic of China

ABSTRACT: Chemical looping with oxygen uncoupling (CLOU) without the coal gasification that limits the efficiency in ordinary chemical looping combustion (CLC) is a very promising approach for CO_2 capture in the combustion of solid fuels. In the present work, the sol–gel-derived $CuO/CuAl_2O_4$ oxygen carrier was evaluated in terms of its ability to release gaseous oxygen in an oxygen-deficient atmosphere and its reactivity with coal in a laboratory-scaled fluidized-bed reactor at 850, 885, 900, 925, and 950 °C. Three typical Chinese coals of different coal ranks, GP coal (anthracite), FG coal (bituminous), and SL coal (lignite), were used as fuels in the CLOU experiments. The effects of the fuel-reactor temperature and coal rank on the carbon conversion rate, combustion efficiency, and CO_2 yield were investigated. Nearly complete conversion of coals was attained. The conversion from carbon to CO_2 can be enhanced if the temperature increases. Meanwhile, the combustion efficiency would be reduced because of the loss of partially unconverted products, such as H_2 and CO, in the reduction process at a higher temperature. Experimental results also suggest that a higher reaction rate but lower combustion efficiency can be attained when the coal of a lower rank is used.

1. INTRODUCTION

Chemical looping combustion (CLC), during which a sequestration-ready CO_2 stream is directly generated from a novel two-step reaction,[1−4] has been considered as a very promising route for high efficiency and low energy consumption concentrating and separating CO_2 from fossil fuel use. In a classical CLC system, oxygen carrier (OC) particles are circulated to carry active lattice oxygen from air in an air reactor (AR) to carbonaceous fuel in a fuel reactor (FR). CLC of gaseous fuels has been successfully demonstrated in many pilot-scaled units of sizes up to 120 kW.[5,6] However, it is challenging to use solid fuels in CLC because of the low rate of reaction between solid fuels and OC. Therefore, several variants of CLC,[7] e.g., syngas-CLC,[8] *in situ* gasification CLC (iG-CLC),[9] and chemical looping with oxygen uncoupling (CLOU),[10] were developed. In syngas-CLC, it is costly to gasify solid fuel with an energy-intensive air separation unit. In iG-CLC, the gasification rate is much lower than the reduction rate, resulting in low coal combustion efficiency (usually, <85%) and low CO_2 capture efficiency (usually, <90%).[11−15] In CLOU, where OC is used to provide gaseous oxygen to react with solid fuels, the reaction rate is much higher than that of iG-CLC.

In CLOU, an OC is required to release and absorb gaseous O_2 repeatedly at combustion temperatures (800−1000 °C), a condition that is significantly different from ordinary CLC technology. A typical schematic of CLOU of coal is shown in Figure 1, where the reaction in the FR can be divided into two steps, i.e., the release of gaseous O_2 from the OC (R1) and the coal combustion with gaseous O_2 (R2). When the OC particles (MeO_x) are introduced into the FR, they will decompose and release gaseous O_2 because, in the high-temperature and oxygen-deficient environment, the partial pressure of O_2 is lower than the equilibrium partial pressure of O_2 over the OC. The reduced OC (MeO_{x-1}) from the FR is then carried back to the AR. Because in the AR, the partial pressure of O_2 is higher than the equilibrium partial pressure of O_2 over the OC, the OC reacts with gaseous O_2 in air to regenerate (see R3). By circulating the OCs between the AR and FR, the CLOU process can run continuously. Therefore, without the rate-limiting gasification step in CLC of solid fuels, the overall reaction rate in the FR is dramatically increased. Gas stream from the FR consists mainly of CO_2 and H_2O, where CO_2 can be concentrated by a simple cooling.

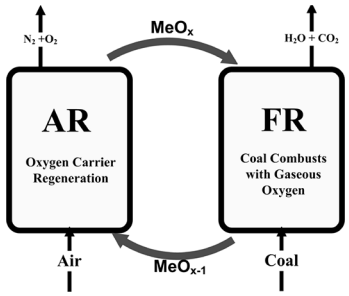

Figure 1. Schematic of CLOU technology.

$$2MeO_x \rightarrow 2MeO_{x-1} + O_2(g) \quad \text{(R1)}$$

$$\text{coal} + O_2(g) \rightarrow CO_2(g) + H_2O(g) \quad \text{(R2)}$$

$$2MeO_{x-1} + O_2(g) \rightarrow 2MeO_x \quad \text{(R3)}$$

Thermodynamically, the Cu-, Mn-, and Co-based metal oxides and some perovskite-type oxides can release and absorb gaseous oxygen at high temperatures of 800−1000 °C.[7,10,16]

Received: December 25, 2012
Revised: April 10, 2013

   dx.doi.org/10.1021/ef3021602 | *Energy Fuels* XXXX, XXX, XXX−XXX

However, only Cu- and Mn-based oxides and some perovskite-type oxides can be used in CLOU.

Arjmand et al.[17] investigated the release of oxygen from the Al_2O_3 and $MgAl_2O_4$-supported CuO OCs and their reactivity with methane. They suggested that Al_2O_3-supported CuO could be used as an OC for CLC processes and $MgAl_2O_4$-supported CuO could be used as an OC for CLOU processes. Adánez-Rubio et al.[18,19] prepared several CuO-based OCs with different CuO contents and different inert supports by impregnation and mechanical mixing. The OCs with 60 wt % CuO on $MgAl_2O_4$ and with 40 wt % CuO on ZrO_2, which were prepared by mechanical mixing, followed by pelletizing by pressure, were highlighted for their best reactivity, attrition, or agglomeration resistance. The corresponding OCs also exhibited excellent characteristics of repeated oxygen release/absorption required for the CLOU process. Mattisson et al.[20] synthesized the CuO/ZrO_2 OC by the freeze granulation method and then investigated the reaction process of the synthetic CuO/ZrO_2 and petroleum coke in a laboratory-scaled fluidized-bed reactor. Leion et al.[21,22] further studied the feasibility of CLOU of six different solid fuels (Mexican petroleum coke, South African coal, Indonesian coal, Colombian coal, German lignite, and Swedish wood char). The OC can release oxygen with an O_2 concentration of 10% at 950 °C in a N_2 atmosphere, and the solid fuels reacted rapidly with oxygen in the atmosphere. The corresponding average carbon conversion rates of the fuels are 3−15 times faster, and the fraction of unconverted combustible gases is significantly lower than that of CLC of solid fuels. Abad et al.[23−25] demonstrated the CLOU process using a spray-drying-derived $CuO/MgAl_2O_4$ (60:40, wt %) as an OC and bituminous coal as fuel in a 1.5 kW_{th} pilot plant. Coal combustion efficiency of nearly 100%, high CO_2 capture efficiency (above 97%), high char conversion in the FR (above 0.94), and fast char conversion rate (7−33%/s) were obtained under a wide range of operating conditions. Besides the synthetic CuO-based OCs, natural copper ore was successfully used for cyclic oxygen release and absorption by Wen et al.[26]

Besides Cu-based OC, the Mn-based metal oxides and perovskite-type oxides were investigated as possible CLOU OCs. Shulman et al.[27] prepared Mn/Fe, Mn/Ni, and Mn/Si oxides and studied their abilities of releasing oxygen and reactivity with methane in a fluidized-bed reactor. The characteristics of oxygen release by iron manganese oxide were further studied by Azimi et al.[28] Solid fuels, such as Colombian coal and petroleum coke, were used in the CLOU system to explore their thermochemical characteristics. Their studies suggested that the fuels can consume the oxygen released from the OC particles effectively. Rydén et al.[29] found that the conversion rate of natural gas was much higher when using the synthetic Mn-based OC than using the Mn ore. The use of perovskite-type oxides ($CaMn_{0.875}Ti_{0.125}O_3$) in CLOU was first introduced by Leion et al.[30] and Rydén et al.[31] In the cycling tests with natural gas, the perovskite-type oxide exhibited a stable physical structure and a good reactivity.

To summarize, the CLOU process is a promising chemical looping technology for the capture of CO_2 from the use of fossil fuels (especially solid fuels, such as coal and petroleum coke). A key factor for the CLOU technology development is a special OC, which may decompose to a reduced metal oxide and gas-phase oxygen in the FR and regenerate itself in the AR. CuO has received a great deal of attention as an efficient OC, because it has some advantageous characteristics, such as high reactivity, high oxygen transport capacity, and suitable equilibrium partial pressure of oxygen at temperatures of interest for combustion (800−1000 °C). It also has stable recyclability, moderate price, good exothermicity for fuel combustion in the FR, and environmental friendliness. In practice, the active component CuO is usually supported by different inert materials, such as ZrO_2, $MgAl_2O_4$, Al_2O_3, SiO_2, MgO, TiO_2, and sepiolite, to withstand a higher temperature (such as 1000 °C) without softening, sintering, agglomeration, and attrition. It is noted that the inert support and the weight ratio of CuO determine the reactivity, stability, resistance to agglomeration, and attrition of the OC to some extent.[18] Among these supports, Al_2O_3 has received considerable attention.

In the case of Al_2O_3 as a support, the $CuAl_2O_4$ spinel is invariably formed at high temperatures (above 1000 °C) by the solid-state reaction (R4), resulting in the partial loss of CuO.

$$CuO + Al_2O_3 \rightarrow CuAl_2O_4 \quad \text{(R4)}$$

However, $CuAl_2O_4$ is not entirely inert, which can be reduced by different fuels (e.g., CO[32] or CH_4[17,33]). Besides, a higher resistance to agglomeration and attrition can be achieved using $CuAl_2O_4$ as a support (which has characteristics of high melting point, good thermal stability, high hardness, and corrosion resistance). Arjmand et al.[17,33] suggested the $CuAl_2O_4$ could be used as an OC for CLC processes because of its resistance against agglomeration/sintering and attrition.

In this paper, the sol−gel-derived OC, combining CuO (60 wt %) and active support $CuAl_2O_4$ (40 wt %), was studied. The process of oxygen release and the reactivity with three typical Chinese coals of different coal ranks were investigated in a laboratory-scaled fluidized-bed reactor. The physicochemical characteristics of the fresh and used OCs were examined. The feasibility of CLOU was demonstrated using three typical Chinese coals as fuels and $CuO/CuAl_2O_4$ as an OC.

2. EXPERIMENTAL SECTION

2.1. OC and Coal Particle Preparation. The sol−gel method has received much attention in catalyst[34] and OC[35−38] preparation because of the high purity and accurate stoichiometry of the products, the homogeneous mixing of components almost at the molecular level, and the microstructure that is controllable using a low-temperature synthesis. Generally, there are four steps in the sol−gel procedure, i.e., the preparation of boehmite γ-AlOOH sol, the preparation of the γ-AlOOH wet gel, the drying of the wet gel, and the heat treatment (calcination). The reagents used in the preparation of the $CuO/CuAl_2O_4$ OC are aluminum isopropoxide [$Al(C_3H_7O)_3$, KESHI Co., 99.9% purity], copper nitrate [$Cu(NO_3)_2{\cdot}3H_2O$, Sinopharm Co., 99.9% purity], and nitric acid (1 mol/L), where copper nitrate and aluminum isopropoxide are precursors for Cu and Al elements in the OC and nitric acid is the catalyst for homogenization. First, the aluminum isopropoxide was ground and dissolved in the deionized water, where the molar ratio of H_2O/Al^{3+} was 100. The $Al(C_3H_7O)_3$ solution was hydrolyzed in a water bath at 85 °C for 1.5 h. Then, HNO_3 (1 mol/L) was added to the solution to attain a H^+/Al^{3+} ratio of 0.07. Afterward, the water bath temperature was raised to 90 °C, at which the solution was aged for 12 h to obtain the boehmite γ-AlOOH sol. Then, $Cu(NO_3)_2$ solution was dispersed into the boehmite γ-AlOOH sol. The resulted mixture was then fully stirred at 90 °C to form the wet gel. The resulting wet gel was dried in an oven step by step (80 °C for 24 h, 100 °C for 5 h, 150 °C for 5 h, and 200 °C for 5 h) to obtain the dried precursor. The resulting $Cu(OH)_2/Al_2O_3$ pieces were calcined under 500 °C for 6 h and under 1000 °C for 10 h in a muffle furnace to produce $CuO/CuAl_2O_4$ pieces. Finally, the conglomeration was ground and sieved to 0.125−0.180 mm to obtain the final OC products.

dx.doi.org/10.1021/ef3021602 | Energy Fuels XXXX, XXX, XXX−XXX

Table 1. Proximate and Ultimate Analyses of Three Coals

	proximate (wt %, ar)				ultimate (wt %, daf)				lower heating value (MJ/kg)
solid fuels	moisture	volatiles	ash	fixed carbon	C	H	N	S	H_{coal}
GP coal	2.25	10.69	20.62	66.44	70.04	3.54	1.90	1.24	26.17
FG coal	1.65	27.19	19.62	51.54	65.54	3.34	1.24	0.80	28.85
SL coal	8.62	41.59	35.47	14.32	48.33	4.11	0.85	0.48	12.82

Chinese coals of three typical coal ranks, including an anthracite from GaoPing (GP coal), a bituminous coal from FuGu (FG coal), and a lignite from ShengLi (SL coal), were selected for CLOU combustion with the $CuO/CuAl_2O_4$ OC. The coals were first dried under 105 °C for 10 h in an oven and then ground and sieved to produce coal particles with a diameter range of 0.20−0.30 mm. The final coal particles were then stored in a drying basin ready for use.

2.2. Characterization of OC and Coal Particles. The fresh and used OC particles were analyzed using a powder X-ray diffraction instrument (Shimadzu, XRD-7000) with Cu Kα radiations under 2θ = 10−90°. The maximum tube voltage and current of the instrument were 40 kV and 30 mA, respectively. The Brunauer−Emmett−Teller (BET) surface area of the $CuO/CuAl_2O_4$ particles was evaluated by the N_2-absorption method (Micromeritics, ASAP2020). The microstructure was examined by a field emission scanning electron microscope (FEI, Sirion). The crushing strength of the fresh OC particles was measured by a force dynamometer (Shimpo, FGJ-5). The average value of 30 randomly selected particles sized within 0.125−0.180 mm is 1.89 N, which is high enough[27] to be used in the fluidized-bed reactor.

The composition and lower heating value of these coals were determined by an ultimate analyzer (Vario, EL-2) and a proximate analyzer (Las Navas, TGA2000), as shown in Table 1.

2. 3. Fluidized-Bed Reactor and Experiments. The schematic of the laboratory-scaled fluidized-bed reactor is shown in Figure 2. The

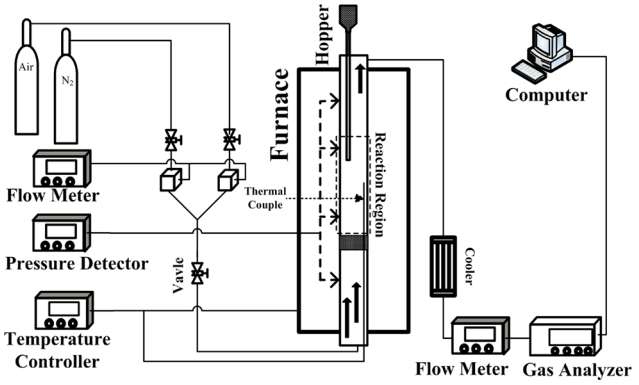

Figure 2. Overview of the fluidized-bed reaction system.

gas control unit provides air or N_2 as the fluidization gas to simulate the AR or FR atmosphere in CLOU. A stainless reaction tube with a length of 892 mm is placed into an electrical furnace. A porous plate with a diameter of 26 mm is placed in the tube at 400 mm from the bottom. The reactor temperature is measured by a type K thermocouple at about 10 mm above the porous plate. The flow rate of the fluidization gas was set at 800 mL/min, so that the inlet gas velocities were 4−9 times the u_{mf}, where u_{mf} is the minimum fluidization velocity. OC particles and coal particles were introduced into the reactor through the hopper on the top of the reactor. All gas products exiting the reactor were first led to an electric cooler to remove the steam and then to a gas analyzer to detect the concentration of CO_2, CO, CH_4, H_2, and O_2, which was further recorded by a computer every second.

In the CLOU experiments of coal, 40 g of OC particles was first exposed to the air for 30 min at a preset temperature to ensure complete oxidation. Then, the fluidization gas was switched rapidly from air to N_2 to simulate the inert atmosphere in FR. The O_2 partial pressure in the tube will drop sharply and then tend to stabilize. A total of 0.3 g of coal particles was added to the hopper and then pushed into the reactor by a pressurized purging nitrogen gas. The coal particles combusted rapidly with the gaseous O_2. The concentrations of gas products (such as CO_2, CO, CH_4, H_2, etc.) were measured by the gas analyzer. When no CO_2 was detected in the exhausted gas, the combustion of the fuel was assumed to be complete. Then, the fluidization gas was switched from N_2 to air. The reduced OC was reoxidized by absorbing O_2 from air. When the O_2 concentration at the reactor exit reached 20.95%, the oxidation process was considered complete. The CLOU experiments of the three coals were carried out at 850−950 °C to investigate the effects of the temperature on the thermochemical characteristics of CLOU using different coals. Finally, the repeated reduction−oxidation ability of the OC was tested in five reduction and oxidation cycles.

2.4. Data Evaluation. Taking into account the scouring of fluidization gas, some fly ash containing carbon was taken away by the exhaust, which was considered as a loss in coal conversion.[39] To address the amount of usable carbon in the fly ash and carbon balance in the reactor, the residual carbon ratio R_C was calculated, which was defined as the molar ratio of carbon in fly ash to the total carbon in the coal. R_C was obtained on the basis of the carbon balance in the system. It is the difference between the carbon flow of coal feed and the total carbonaceous gas flow leaving the reactor. Because no carbon-containing substances were detected in the oxidation process, R_C was calculated by considering the reduction process only

$$R_C = 1 - \frac{\int_{t_0}^{t_{total}} V_{flus}(C_{CO} + C_{CO_2} + C_{CH_4})dt}{n_{C,coal}} \quad (1)$$

where t_0 and t_{total} represent the start and end times of the whole reduction, C_{CO}, C_{CO_2}, and C_{CH_4} are the molar fractions of CO, CO_2, and CH_4 at each second in the gas products (dry basis), respectively, $n_{C,coal}$ is the molar amount of carbon in the coals, and V_{flus} (mol/s) represents the molar flow rate of the gas products, which is obtained from N_2 balance in the fluidization gases entering and leaving the reactor.

The mass of carbon in the fly ash, $m_{C,fly\ ash}$, can be calculated by eq 2.

$$m_{C,fly\ ash} = R_C m_{C,coal} \quad (2)$$

In eq 2, $m_{C,coal}$ is the mass of carbon in the coal, $m_{C,coal} = f_C m_{coal}$, f_C is the mass fraction of the element C in the coal, as shown in Table 1, and m_{coal} is the mass of coal added to the reactor.

The conversion of combustible carbon in reduction, $X_{C,comb}$, can be estimated by eq 3.

$$X_{C,comb} = \frac{\int_{t_0}^{t} V_{flus}(C_{CO} + C_{CO_2} + C_{CH_4})dt}{\int_{t_0}^{t_{total}} V_{flus}(C_{CO} + C_{CO_2} + C_{CH_4})dt} \quad (3)$$

All carbon-containing gases (CO_2, CO, and CH_4) in the period of t_0−t_{total} of the reduction were considered in eq 3. At the end of the reduction, the conversion rate of combustible carbon is 1.

The average carbon conversion rate X_{Cavg} (%/s) was estimated by eq 4 to measure the reaction rate in the FR.

$$X_{Cavg} = \frac{X_{C,comb}}{t - t_0} \times 100\% \quad (4)$$

dx.doi.org/10.1021/ef3021602 | Energy Fuels XXXX, XXX, XXX−XXX

In this paper, the time $t_{0.95}$ when 95% of combustible carbon was converted and the average carbon conversion rate $X_{Cavg,0.95}$ were calculated to investigate the effect of the temperature on the reaction process.

By considering the carbon in the fly ash, the coal combustion efficiency (η_{eff}) was estimated by eq 5, in which CH_4, CO, and H_2 in the flue gas and residual carbon in the fly ash were considered as a thermal loss.

$$\eta_{eff} = 1 - (H_{CO}\int_{t_0}^{t_{total}} M_{CO}V_{flus}C_{CO}dt + H_{CH_4}\int_{t_0}^{t_{total}} M_{CH_4}V_{flus}C_{CH_4}dt + H_{H_2}\int_{t_0}^{t_{total}} M_{H_2}V_{flus}C_{H_2}dt + H_C m_{C,fly\ ash})/(m_{coal}H_{coal}) \quad (5)$$

In eq 5, H_{CO}, H_{CH_4}, H_{H_2}, H_C, and H_{coal} (MJ/kg) are the lower heating values of CO, CH_4, H_2, carbon, and coal, respectively, and M_{CO}, M_{CH_4}, and M_{H_2} (kg/mol) represent the molar mass of CO, CH_4, and H_2.

The carbon to CO_2 yield γ_{CO_2}, which was used to reflect the conversion from fuel to CO_2, was calculated by eq 6, considering the total carbon detected in the reduction.

$$\gamma_{CO_2} = \frac{C_{CO_2}}{C_{CO} + C_{CO_2} + C_{CH_4}} \quad (6)$$

3. RESULTS

3.1. Oxygen Release during Gas Switching. The release of oxygen from $CuO/CuAl_2O_4$ was first examined in the fluidized-bed reactor. After switching fluidization gas from air to N_2, the O_2 partial pressure dropped quickly to be lower than the equilibrium O_2 partial pressure. At this moment, the fresh or reoxidated OC released gaseous O_2. As shown in Figure 3,

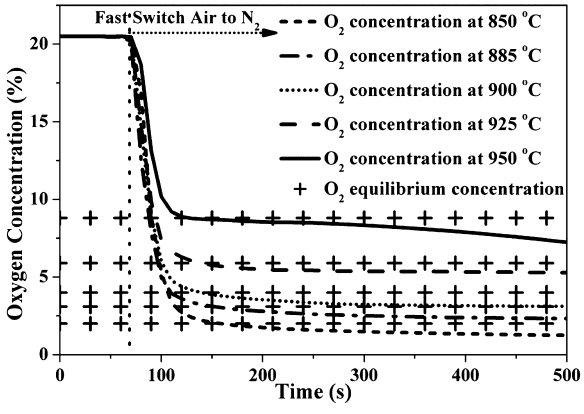

Figure 3. Stable oxygen concentrations under various temperatures.

stable oxygen concentrations can be attained in a N_2 atmosphere at different temperatures. The stable O_2 concentration is a function of the reactor temperature. The higher the temperature, the higher the stable O_2 concentration. The O_2 pressure at the reactor exit is always lower than the corresponding equilibrium O_2 partial pressure over the CuO/Cu_2O system. As known, the O_2 concentration of the AR exhaust has to be higher than the equilibrium O_2 partial pressure at the temperature. Temperatures lower than 950 °C might be the most appropriate for an efficient CLOU process because too high of an excess air ratio is not favored.

The oxygen release tests were also run to determine when to add the coal particles into the reactor. As shown in Figure 3, all of the oxygen release durations are longer than 400 s, which is far longer than the reaction time in CLOU of coals (section 3.2). It is obvious that there is excess oxygen released from the OC in CLOU of coals. When the oxygen concentration stabilizes (usually, 100 s after switching the atmospheric gas), the coal particles were added to the reactor.

The phase analysis of the fresh and used OCs are shown in Table 2. In the fresh OC, no Al_2O_3 was found and $CuAl_2O_4$ was

Table 2. Composition of the OC

fresh	after oxygen release reaction[a]	after regeneration
CuO and $CuAl_2O_4$	Cu_2O, $CuAlO_2$, CuO[m], and $CuAl_2O_4$[m]	CuO and $CuAl_2O_4$

[a]m = minor phase.

generated because of the interaction between CuO and Al_2O_3. A similar finding was reported by Chuang et al.[32] After the release of oxygen, CuO and $CuAl_2O_4$ in the fresh OC were converted to Cu_2O and $CuAlO_2$, respectively. There exist small amounts of $CuAl_2O_4$ and CuO because of the incomplete decomposition of active phases. After reoxidation, the CuO and $CuAl_2O_4$ phases were restored (again, no Al_2O_3 was found).

3.2. Reaction with Three Typical Coals. *3.2.1. Reaction Profiles.* A typical gas concentration profile when using FG coal as fuel in CLOU at 950 °C is shown in Figure 4. The oxygen

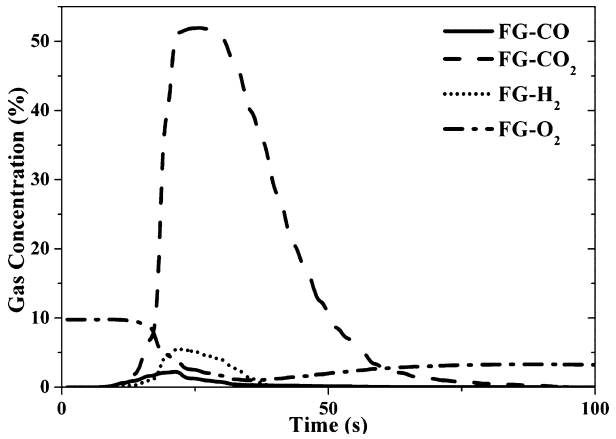

Figure 4. Reaction profile for FG coal at 950 °C.

concentration decreases sharply from 9.8 to 1% within 30 s when the FG coal is introduced into the reactor, because of a large amount of O_2 consumed in coal combustion. The CO_2 concentration increases sharply up to 52% within 30 s, suggesting that the reaction between coal and gaseous O_2 is rapid. A small amount of CO and H_2 is detected in the beginning of the reduction period, which is due to the devolatilization of the coal particles. Such combustible gas does not react with the gaseous O_2 completely before leaving the reactor because of the lack of time. It is noted that the concentrations of H_2, CO, and CH_4 are lower than 6.0, 2.0, and 0.1%, respectively (shown in Figure 4), and the durations of the combustible gas are usually less than 40 s. When no carbon-containing species was detected in the outlet gas from the reactor, the fluidization gas was switched from N_2 to air to simulate the AR atmosphere in CLOU. In the following oxidation process, O_2 concentrations at the reactor exit increased gradually to 20.95% and no carbon-containing gas was detected in the reactor outlet, suggesting that all of the coal

dx.doi.org/10.1021/ef3021602 | Energy Fuels XXXX, XXX, XXX−XXX

particles were converted and no carbon deposited on the surface of OC particles in the reduction process. Similar patterns for other coals were observed, as shown in Figure 5 for

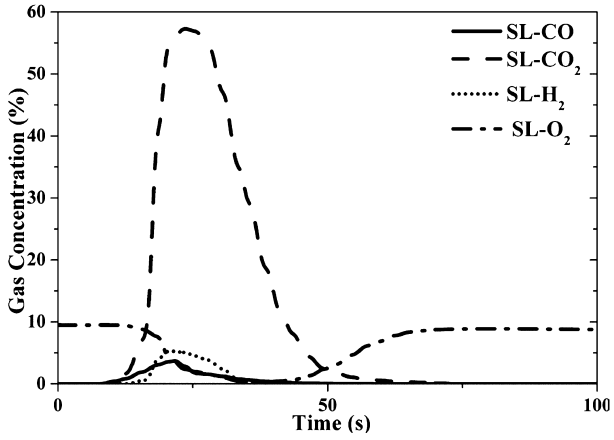

Figure 5. Reaction profile for SL coal at 950 °C.

SL coal and Figure 6 for GP coal. The patterns of the reaction profiles at other temperatures (850, 885, 900, and 925 °C) for different coals are similar to that shown in Figures 4–6 at 950 °C.

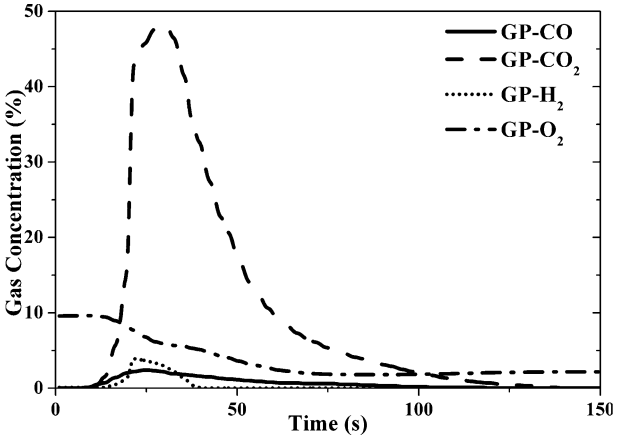

Figure 6. Reaction profile for GP coal at 950 °C.

3.2.2. Conversion of Combustible Carbon in the Coals. We defined the carbon conversion rates for FG, GP, and SL coals as $X_{C,comb,FG}$, $X_{C,comb,GP}$, and $X_{C,comb,SL}$, respectively. Because the amount of combustible carbon was estimated by the total carbon consumption in the reduction, the conversion rates of the combustible carbon varied between 0 and 1 in the reduction process, as shown in Figure 7 for GP coal for example. The conversion rates of the combustible carbon, $dX_{C,comb}/dt$, are different at different temperatures for different coals. With the temperature increasing from 850 to 950 °C, the maximum rate of carbon conversion of GP coal increases from 0.5 to 4.3%/s (as shown in Figure 8) and the maximum rates of carbon conversion of FG coal and SL coal increase from 1.5 to 6.2%/s and from 3.5 to 8%/s, respectively. Obviously, a higher temperature can increase the carbon conversion rate in the reduction process. The carbon conversion rate also depends upon the coal rank. As shown in Figure 9, at the same temperature (900 °C), the carbon conversion rate of SL coal (lignite) is the highest, which is 2 times that of FG bituminous

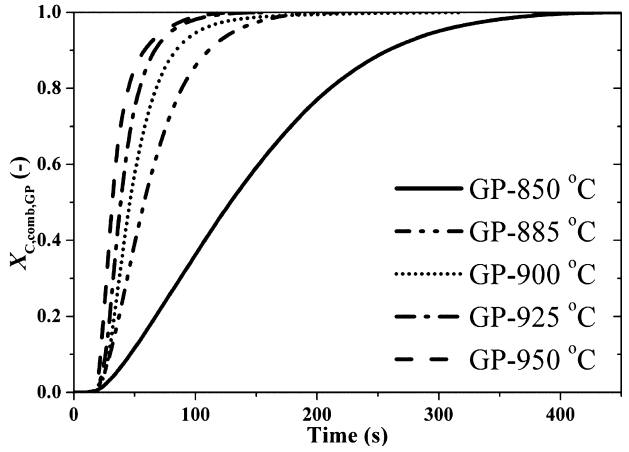

Figure 7. Carbon conversion for GP coal at various temperatures.

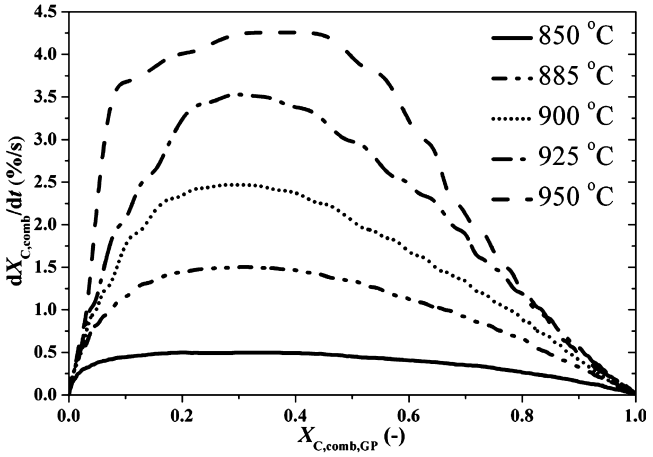

Figure 8. Conversion rate of combustible carbon for GP coal at various temperatures.

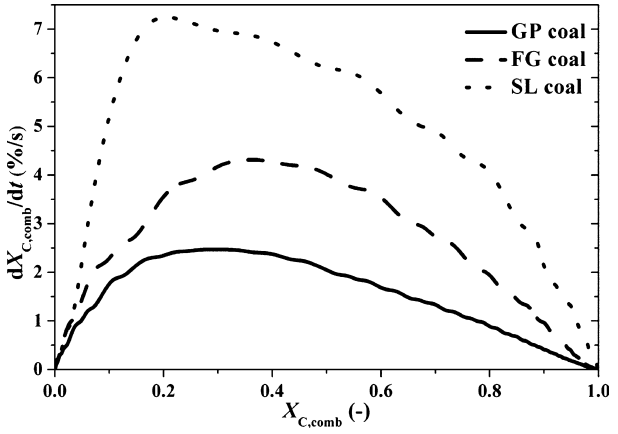

Figure 9. Conversion rate of combustible carbon for different coals at 900 °C.

coal and 3.5 times that of GP coal (anthracite). The lower the coal rank, the higher the carbon conversion rate.

3.2.3. Effects of the Temperature. The time ($t_{0.95}$) required for 95% conversion of the fuel and the average rate ($X_{Cavg,0.95}$) of combustion during the period were calculated, as shown in Figures 10 and 11, respectively. $t_{0.95}$ decreases with the reactor temperature (see Figure 10). The average carbon conversion

dx.doi.org/10.1021/ef3021602 | Energy Fuels XXXX, XXX, XXX–XXX

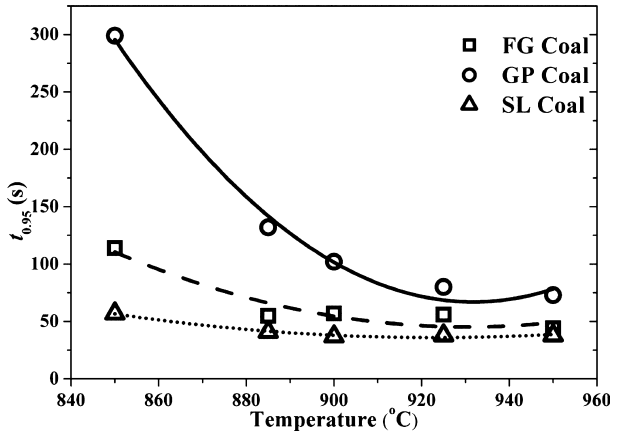

Figure 10. Effects of the temperature and volatiles on the characteristic reaction time.

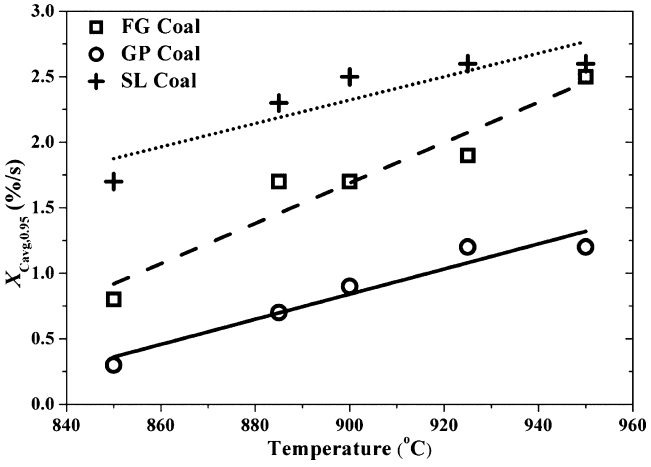

Figure 11. Effects of the temperature and volatiles on the average carbon conversion rate.

rate ($X_{Cavg,0.95}$) increases with the reactor temperature (see Figure 11). It is noted that, the higher the coal rank, the greater the changes in the time $t_{0.95}$. The temperature effect is related to two factors: the carbon content and the volatile content in the coals. After being heated, the coal will decompose to char and volatiles. Two types of reactions occur in the FR, i.e., the solid−gas reaction between char and the gaseous O_2 and the gas−gas reaction between volatiles and O_2. However, the solid−gas reaction is much slower than the gas−gas reaction.[40] Among the three coals, the GP coal has the highest content of fixed carbon and the least volatile content. A higher temperature favors the combustion of coke in the GP coal and, thereby, increases the combustion rate to a greater extent.

On the other hand, a higher temperature also increases the release of volatiles, which may not be conducive to the complete combustion of the fuel in the fluidized-bed reactor because of insufficient residence time of combustible gases. The total amount of the escaped combustible gases, i.e., CO, H_2, and CH_4, for each coal at various temperatures was estimated by the integral in the whole reduction period, as shown in Table 3. Generally, the total amount of CO and H_2 increases with the increase of the temperature. The effects of the temperature on the maximum concentration of these gases in the outlet are similar, as shown in Table 4, suggesting that a higher temperature is not conducive to the generation of pure CO_2.

Table 3. Total Amount of Combustible Gases in the Outlet of the Reactor

		temperature (°C)				
gas amount (mmol)	coals	850	885	900	925	950
CO	GP	0.11	1.03	0.97	0.89	0.95
	FG	0.58	0.44	0.45	1.71	5.65
	SL	0.42	0.46	0.46	0.65	1.79
H_2	GP	0.15	0.21	0.49	0.62	0.72
	FG	0.38	0.43	0.64	1.37	1.55
	SL	0.64	0.62	0.72	1.30	1.25

Table 4. Maximum Concentration of Combustible Gases in the Outlet of the Reactor

		temperature (°C)				
maximum concentration (%)	coals	850	885	900	925	950
CO	GP	0.1	1.7	1.9	2.0	2.4
	FG	4.18	3.6	3.54	10.07	22.4
	SL	3.35	3.45	3.03	3.62	9.66
H_2	GP	0.6	1.2	2.4	3.1	3.9
	FG	2.5	3.2	4.1	6.2	5.5
	SL	3.8	4.1	4.8	5.8	5.6

Besides these escaping combustible gases, the carbon in fly ash also leads to the extra loss of combustible components. Carbon residue ratio R_C is about 0.03 for each type of coal. These residual carbons escape from the reactor with fly ash rather than sticking to the inner surface of the reaction tube because there were no carbon-containing gases detected in the oxidation process. The combustible gases (CO, H_2, and a small amount of CH_4) in the outlet and the residual carbon in fly ash were considered as a heat loss, which decreased the combustion efficiency. Figure 12 shows the combustion efficiency of these coals at various temperatures. The combustion efficiency of SL coal is the lowest and varies in the range of 0.75−0.91. The FG coal has the highest combustion efficiency at the temperatures of lower than 900 °C. However, it decreases quickly when the temperature is higher than 900 °C. In comparison to FG coal and SL coal, the GP coal has steady combustion efficiency. A

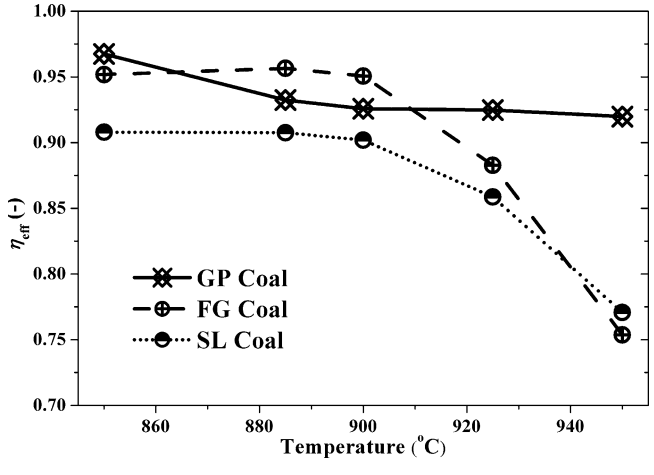

Figure 12. Effects of the temperature on combustion efficiency.

dx.doi.org/10.1021/ef3021602 | Energy Fuels XXXX, XXX, XXX−XXX

higher temperature above 900 °C is not conducive to efficient combustion of these coals with high volatile contents (FG coal and SL coal) because at higher temperatures more combustible gases escape from the reactor. It is expected that, in a real CLOU unit of an interconnected fluidized-bed reactor, the combustion efficiency of these coals could be improved because of the higher use rate of volatiles in the coals. For example, in the work by Adánez-Rubio et al.,[41] a continuous CLOU system was used to test the $CuO/MgAl_2O_4$ OC. For the similar coals, the volatiles in the coals were completely combusted in their studies, which resulted in high combustion efficiencies (~100%). Because of the efficient use of volatiles, the temperature has little effect on the variation of combustion efficiency.

The carbon to CO_2 yield during the reduction was shown as a function of time in Figure 13. Initially, the value of γ_{CO_2} increases quickly to close to 1 because of the fast combustion of carbon in the coals. After that, a stable yield from carbon to CO_2 was attained. It is noted that the temperature influences the conversion rates of carbon to some extent. A higher γ_{CO_2} can be obtained at a lower temperature, because of the smaller amount of volatiles escaping from the reactor.

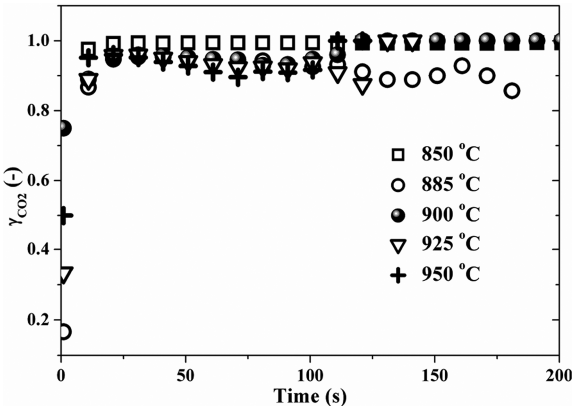

Figure 13. CO_2 yield for GP coal at various temperatures.

3.2.4. Cycling Tests with Three Coals. Successive reduction−oxidation cycles were carried out at 900 °C to study the potential cyclic stability of the $CuO/CuAl_2O_4$ OC in CLOU of coals. Figure 14 shows the gas concentration profiles in five redox tests at 900 °C using GP coal as fuels. In the reduction period, the CO_2 concentration varies in the range of 14−18% and the time required in each reduction is about 0.5 h. In addition, about 0.1% CO and 0.3−0.4% H_2 were detected in the cyclic tests (not shown in Figure 14). The oxygen concentration remains stable at 2% in the reduction period and increases rapidly to 20.95% in the oxidation period. With the increase of the cycle number, the concentration of CO_2 decreases slightly, suggesting that a little decline of the reactivity of the OC might exist. The gas concentration profiles of combusting FG coal and SL coal are similar (not shown); however, the CO_2 and combustible gas (H_2 and CO) concentrations are higher, and the reaction time is shorter. Among the three coals, it takes about 3, 2.2, and 1.4 h to complete the five cycles for combusting GP coal, FG coal, and SL coal, respectively.

Combustion efficiencies of the three coals are displayed in Figure 15. For all three coals, the combustion efficiency is higher than 90% but fluctuates with the cyclic number because of experimental errors and a slight reactivity attenuation of OC. The highest combustion efficiency was obtained for GP coal in the first cycle, which was higher than 97%. In addition, the GP

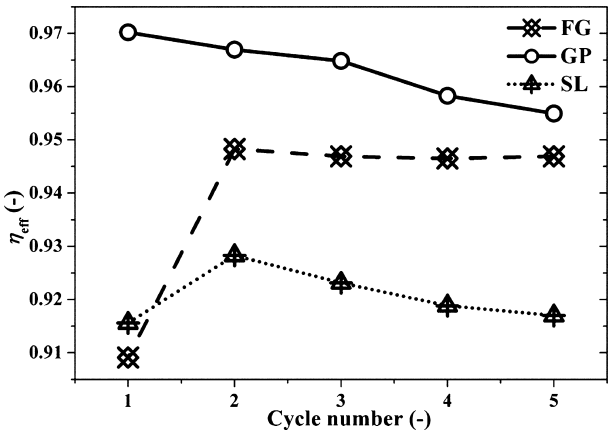

Figure 15. Combustion efficiency for each coal at 900 °C.

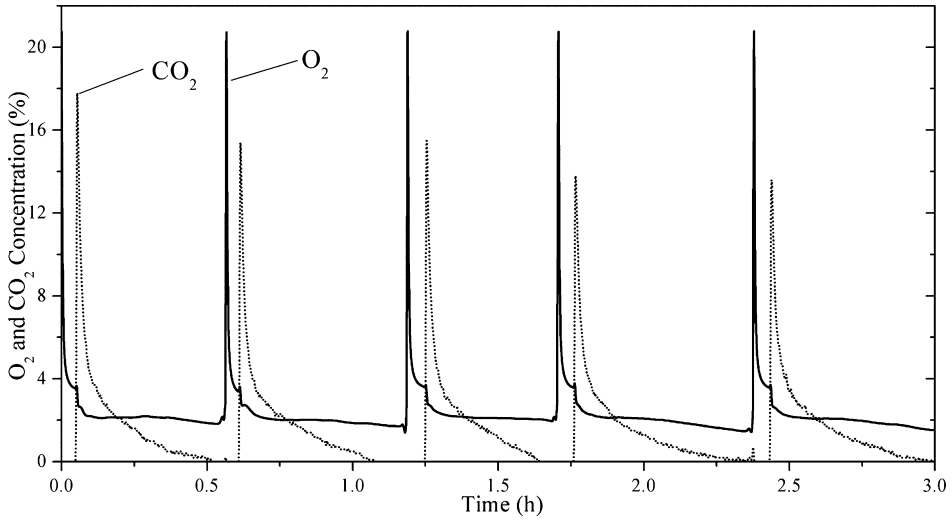

Figure 14. Cycling tests for the OC with GP coal at 900 °C.

dx.doi.org/10.1021/ef3021602 | *Energy Fuels* XXXX, XXX, XXX−XXX

coal with less amount of volatile attains a higher CO_2 yield in all of the cyclic tests (Figure 16). A stable CO_2 yield for GP coal is

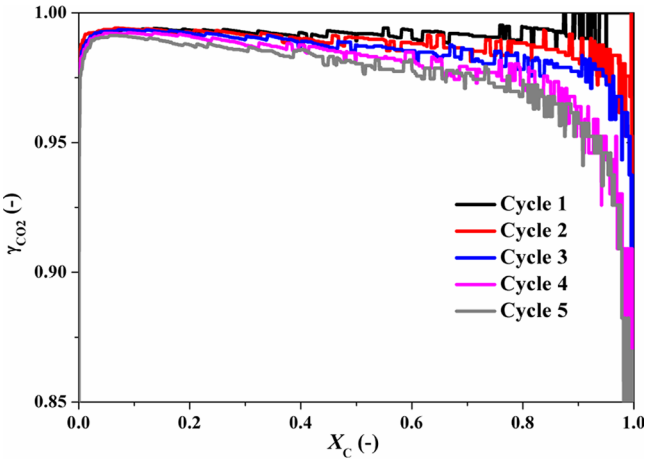

Figure 16. CO_2 yield for GP coal at 900 °C.

higher than 0.90, suggesting that efficient conversion from carbon to CO_2 can be achieved. However, with the increase of the cycle number, a slight decline of γ_{CO_2} can be observed, which suggests that the reactivity of OC decreases slightly with the increase of the cycle number.

3.2.5. Pore Structure and Surface Morphology Analysis. The results of BET analysis for the fresh and used OCs in the CLOU process of the three coals are summarized in Table 5.

Table 5. Pore Structure Analysis of the OC Particles

	BET area ($\times 10^3$, m^2/kg)	pore volume (cm^3/kg)	BJH adsorption pore diameter (nm)
fresh OC	1.06	5.29	58.9
used with GP coal	0.18	0.35	82.9
used with FG coal	0.13	0.27	91.6
used with SL coal	0.17	0.38	89.6

The BET area of the fresh OC is 1.06×10^3 m^2/kg, and the pore volume is 5.29 cm^3/kg. The used OC with the three coals has smaller BET areas and pore volumes, probably because of the blocking of fly ash generated in the coal combustion process and a slight sintering in the OC particle. Although the OC has a relatively small BET area and pore volume, the reactivity is maintained well because the release of oxygen is a nucleation and nuclei growth process[42] (implying that the release of oxygen does not fully depend upon the surface structure of the particles). When the OC is reoxidated, following the cyclic reactions with the three coals, XRD analysis revealed the presence of CuO and $CuAl_2O_4$ in the particles, and no other minor phase was detected. The crushing strength of the OC particles used in the cycle tests was 1.50 N, which is lower than that of the fresh particles (1.89 N), suggesting that the mechanical characteristic decreases after being used repeatedly in the tests. In the multi-redox with different coals, no agglomeration of the OC particles has been observed, judging from the microstructures as shown in Figure 17.

4. CONCLUSION

$CuO/CuAl_2O_4$, which is able to release oxygen at oxygen-deficient atmospheres (e.g., when being fluidized by N_2) and at suitable temperatures, could be used as a potential OC for CLOU. Three types of Chinese coals of different coal ranks, including GP coal (anthracite), FG coal (bituminous), and SL coal (lignite), can be nearly completely converted in the CLOU tests using $CuO/CuAl_2O_4$ as an OC. No carbon-containing gases were detected in the oxidation period, and the residual carbon ratio is only 0.03 for each coal on the basis of the carbon balance in the system. A higher temperature can enhance the carbon conversion. The time $t_{0.95}$ required for 95% conversion of coals decreases gradually to a nearly stable value with the increase of the temperature, and the average carbon conversion rate increases with the temperature. It is also found that the carbon conversion rate is higher when combusting a coal with a lower coal rank at the same temperature; higher temperatures can increase the reaction rate of high-rank coal to a greater extent because a higher temperature favors the combustion of char of high-rank coal (e.g., GP coal). On the other hand, a higher temperature also favors the pyrolysis and volatilization of coals and, thereby, is not conducive to the complete combustion because, in the laboratory fluidized-bed reactor, the combustible gases released from coals do not react with the gaseous O_2 completely before leaving the reactor as a result of the lack of time.

Combustion efficiency decreases slightly with the cycle numbers in the successive reduction−oxidation tests, which suggests that the reactivity of the $CuO/CuAl_2O_4$ OC decreases slightly in the redox tests. Therefore, the reactivity stability of the $CuO/CuAl_2O_4$ OC needs to be improved to be used in continuously operating units, such as pilot plants.

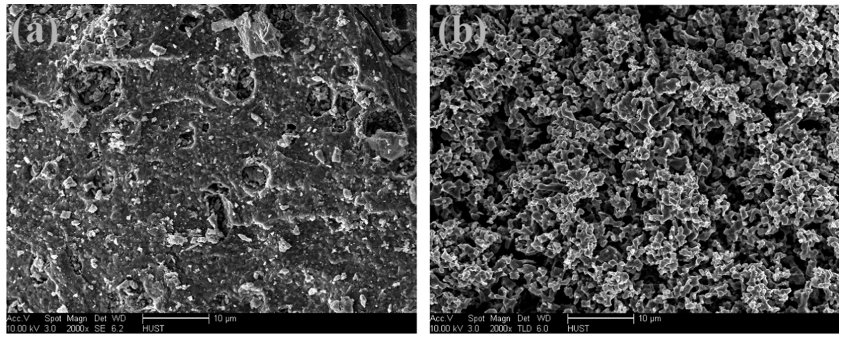

Figure 17. Microstructure of (a) fresh OC and (b) used OC in the CLOU tests.

dx.doi.org/10.1021/ef3021602 | *Energy Fuels* XXXX, XXX, XXX−XXX

AUTHOR INFORMATION

Corresponding Author

*Telephone: +86-27-8754-4779, ext. 8208. Fax: +86-27-8754-5526. E-mail: klinsmannzhb@163.com.

Notes

The authors declare no competing financial interest.

ACKNOWLEDGMENTS

These authors were supported by the "Program for New Century Excellent Talents in University (NCET-10-0395)", the "National Natural Science of China (50936001 and 51021065)", and the "National Basic Research Program (2010CB227004)". Meanwhile, the staff from the Analytical and Testing Center, HUST, are also appreciated for the related experimental analysis. Ho Simon Wang at HUST Academic Writing Center has provided tutorial assistance to improve the manuscript.

REFERENCES

(1) Lewis, W. K.; Newton; Gilliland, E. R. U.S. Patent 2,665,972, 1954.
(2) Figueroa, J. D.; Fout, T.; Plasynski, S.; McIlvried, H.; Srivastava, R. D. *Int. J. Greenhouse Gas Control* **2008**, *2*, 9−20.
(3) Mattisson, T.; Lyngfelt, A.; Cho, P. *Fuel* **2001**, *80*, 1953−1962.
(4) de Diego, L. F.; García-Labiano, F.; Adánez, J.; Gayán, P.; Abad, A.; Corbella, B. M.; Palacios, J. M. *Fuel* **2004**, *83*, 1749−1757.
(5) Kolbitsch, P.; Bolhàr-Nordenkampf, J.; Pröll, T.; Hofbauer, H. *Int. J. Greenhouse Gas Control* **2010**, *4*, 180−185.
(6) Bolhàr-Nordenkampf, J.; Pröll, T.; Kolbitsch, P.; Hofbauer, H. *Energy Procedia* **2009**, *1*, 19−25.
(7) Adánez, J.; Abad, A.; García-Labiano, F.; Gayán, P.; de Diego, L. F. *Prog. Energy Combust. Sci.* **2012**, *38*, 215−282.
(8) Jin, H.; Ishida, M. *Fuel* **2004**, *83*, 2411−2417.
(9) Cao, Y.; Pan, W. P. *Energy Fuels* **2006**, *20*, 1836−1844.
(10) Mattisson, T.; Lyngfelt, A.; Leion, H. *Int. J. Greenhouse Gas Control* **2009**, *3*, 11−19.
(11) Berguerand, N.; Lyngfelt, A. *Fuel* **2008**, *87*, 2713−2726.
(12) Shen, L.; Wu, J.; Xiao, J. *Combust. Flame* **2009**, *156*, 721−728.
(13) Shen, L.; Wu, J.; Gao, Z.; Xiao, J. *Combust. Flame* **2009**, *156*, 1377−1385.
(14) Shen, L.; Gao, Z.; Wu, J.; Xiao, J. *Combust. Flame* **2010**, *157*, 853−863.
(15) Song, T.; Shen, L.; Xiao, J.; Chen, D.; Gu, H.; Zhang, S. *Combust. Flame* **2012**, *159*, 1286−1295.
(16) Moghtaderi, B. *Energy Fuels* **2010**, *24*, 190−198.
(17) Arjmand, M.; Azad, A. M.; Leion, H.; Lyngfelt, A.; Mattisson, T. *Energy Fuels* **2011**, *25*, 5493−5502.
(18) Adánez-Rubio, I.; Gayán, P.; García-Labiano, F.; de Diego, L. F.; Adánez, J.; Abad, A. *Energy Procedia* **2011**, *4*, 417−424.
(19) Gayán, P.; Adánez-Rubio, I.; Abad, A.; de Diego, L. F.; García-Labiano, F.; Adánez, J. *Fuel* **2012**, *96*, 226−238.
(20) Mattisson, T.; Leion, H.; Lyngfelt, A. *Fuel* **2009**, *88*, 683−690.
(21) Leion, H.; Mattisson, T.; Lyngfelt, A. *Energy Procedia* **2009**, *1*, 447−453.
(22) Leion, H.; Mattisson, T.; Lyngfelt, A. *Oil Gas Sci. Technol.* **2011**, *66*, 201−208.
(23) Abad, A.; Adánez-Rubio, I.; Gayán, P.; García-Labiano, F.; de Diego, L. F.; Adánez, J. *Int. J. Greenhouse Gas Control* **2012**, *6*, 189−200.
(24) Adánez-Rubio, I.; Gayán, P.; Abad, A.; de Diego, L. F.; García-Labiano, F.; Adánez, J. *Energy Fuels* **2012**, *26*, 3069−3081.
(25) Adánez-Rubio, I.; Abad, A.; Gayán, P.; de Diego, L. F.; García-Labiano, F.; Adánez, J. *Fuel* **2012**, *102*, 634−645.
(26) Wen, Y.; Li, Z.; Xu, L.; Cai, N. *Energy Fuels* **2012**, *26*, 3919−3927.
(27) Shulman, A.; Cleverstam, E.; Mattisson, T.; Lyngfelt, A. *Energy Fuels* **2009**, *23*, 5269−5275.
(28) Azimi, G.; Leion, H.; Mattisson, T.; Lyngfelt, A. *Energy Procedia* **2011**, *4*, 370−377.
(29) Rydén, M.; Lyngfelt, A.; Mattisson, T. *Energy Procedia* **2011**, *4*, 341−348.
(30) Leion, H.; Larring, Y.; Bakken, E.; Bredesen, R.; Mattisson, T.; Lyngfelt, A. *Energy Fuels* **2009**, *23*, 5276−5283.
(31) Rydén, M.; Lyngfelt, A.; Mattisson, T. *Int. J. Greenhouse Gas Control* **2011**, *5*, 356−366.
(32) Chuang, S. Y.; Dennis, J. S.; Hayhurst, A. N.; Scott, S. A. *Combust. Flame* **2008**, *154*, 109−121.
(33) Arjmand, M.; Azad, A. M.; Leion, H.; Mattisson, T.; Lyngfelt, A. *Ind. Eng. Chem. Res.* **2012**, *51*, 13924−13934.
(34) Brinker, C. J.; Scherer, G. W. *Sol−Gel Science*; Academic Press: San Diego, CA, 1990; pp 2−9.
(35) Ishida, M.; Jin, H.; Okamoto, T. *Energy Fuels* **1996**, *10*, 958−963.
(36) Zhao, H.; Liu, L.; Wang, B.; Xu, D.; Jiang, L.; Zheng, C. *Energy Fuels* **2008**, *22*, 898−905.
(37) Li, F.; Kim, H. R.; Sridhar, D.; Wang, F.; Zeng, L.; Chen, J.; Fan, L. S. *Energy Fuels* **2009**, *23*, 4182−4189.
(38) Kierzkowska, A. M.; Bohn, C. D.; Scott, S. A.; Cleeton, J. P.; Dennis, J. S.; Müller, C. R. *Ind. Eng. Chem. Res.* **2010**, *49*, 5383−5391.
(39) Shen, L.; Wu, J.; Gao, Z.; Xiao, J. *Combust. Flame* **2010**, *157*, 934−942.
(40) Chapman, S.; Cowling, T. G. *The Mathematical Theory of Non-uniform Gases: An Account of the Kinetic Theory of Viscosity, Thermal Conduction and Diffusion in Gases*; Cambridge University Press: Cambridge, U.K., 1970; pp 159−166.
(41) Adánez-Rubio, I.; Abad, A.; Gayán, P.; de Diego, L. F.; García-Labiano, F.; Adánez, J. *Int. J. Greenhouse Gas Control* **2013**, *12*, 430−440.
(42) Hossain, M. M.; de Lasa, H. I. *Chem. Eng. Sci.* **2010**, *65*, 98−106.